International Journal of Technology 13(2) 398-409 (2022)
Received December 2020 / Revised December 2020 / Accepted November 2021

International Journal of Technology

http://ijtech.eng.ui.ac.id

Characterization and Equilibrium Study of Drug Release of pH-Responsive Chitosan-graft-Maleic Film

Daniel Timotius[1,3], Yuni Kusumastuti[1,2*], Rochmadi[1]

[1]*Department of Chemical Engineering, Universitas Gadjah Mada, Jl. Grafika 2 Yogyakarta 55281, Indonesia*
[2]*Bioresource Engineering Group, Department of Chemical Engineering, Universitas Gadjah Mada, Jl. Grafika 2 Yogyakarta 55281, Indonesia*
[3]*Department of Chemical Engineering, Universitas Pembangunan Nasional "Veteran" Yogyakarta, 55283, Indonesia*

Abstract. This paper reports on a pH responsive material and a mathematical model for a drug release study. This material can be applied as a tumor drug carrier, because the tumor tissue has a different pH (5.7–7.8) compared to the healthy tissue (7.3–7.4). Maleic anhydride (MA) is introduced into the chitosan (CTS) backbone to create a polyampholyte chitosan-graft-maleic (CgM) film that has a pH responsive property. The success of the reaction is confirmed by Fourier transform infrared spectroscopy, which shows a new peak at 1705cm^{-1}. The acidic content and mechanical strength of the material increase with the MA:CTS ratio. Our result shows that the pH responsive property of this material appears at a ratio of 4:2 (weight MA/weight CTS). The equilibrium swelling ratio provides information regarding the isoelectric point, which is obtained at pH 6. The drug release study involves adsorption isotherms and moving boundaries cases. Our calculation results show that the $\boldsymbol{D_e}$ value varies from 2.71 × 10^{-7} to 6.37 × 10^{-7} cm^2/min. The Henry constants vary by approximately 10^2 to 10^3 in the order of magnitude. The Langmuir maximum adsorption capacity is approximately 10^0 to 10^2 mmol/g in the order of magnitude.

Keywords: Adsorption isotherm; Chitosan-graft-maleic; Mathematical model; Moving boundary; pH-responsive

1. Introduction

Recently, the development of biomaterials has shifted from active materials to "smart" materials. These smart materials can respond or adjust depending on their environment (Zhang et al., 2019). In the field of drug delivery systems, several stimuli are used, such as radiation intensity, temperature, enzyme, magnetic field, and pH (Qian et al., 2019). Among these, pH is the most interesting because the human body naturally has a wide range of pH values of approximately 2–7.4 (Manga & Jha, 2017). This stimulus has specific values in different biological conditions; for example, in tumor tissue, the pH value is approximately 5.7–7.8, which is different from that in normal tissue (approximately 7.3–7.4) (Qian et al., 2019). Hence, drug release is expected to be specific to the tumor tissue rather than the healthy tissue.

The pH-responsive drug delivery system commonly uses hydrogel technology.

*Corresponding author's email: yuni_kusumastuti@ugm.ac.id, Tel. +62274-555320
doi: 10.14716/ijtech.v13i2.4594

However, to obtain a pH-responsive hydrogel, the hydrogel should be formed of a polyampholyte, which exhibits different swelling behaviors depending on the pH value and salt concentration of the environment (Su & Okay, 2017). This property is attributed to the presence of anionic and cationic functional groups along the polymer chains. As polyampholyte has both types of charges, the density of each charge type is important. The charge density is affected by the salt concentration or the pH of the environment. When the environment is acidic, the cationic functional groups have a higher density, while in basic media, the density of the anionic functional groups is higher. There is a pH point at which both functional groups have the same density, which is called the isoelectric point (IEP) (Kono et al., 2013). Thus, a polyampholyte can be synthesized from cationic or anionic polymers.

Chitosan (CTS), (1-4)-2-amino-2-deoxy-β-D-glucan, is known as a natural polycationic saccharide (Kusumastuti et al., 2017a) and the second most abundant polysaccharide after cellulose (Muharam et al., 2015). It can be safely used as a raw biomaterial (Wibowo et al., 2021), owing to its properties such as biocompatibility, biodegradation, nontoxicity, and the ability to mimic the native properties of a tissue (Morgado et al., 2015). CTS also exhibits a suitable film-forming ability (Timotius et al., 2020). Therefore, it is reasonable to use CTS as a raw material to build 2D hydrogels. Because CTS is polycationic, it needs to be modified to obtain polyampholyte properties. Hasipoglu et al. (2005) modified CTS with maleic acid through grafting copolymerization by using ceric ammonium nitrate as the initiator. This resulted in chitosan-graft-maleic (CgM), which acts as a polyampholyte. Zhou et al. (2017) grafted maleic anhydride (MA) into CTS without any initiator and further used it as a potential wound dressing. In our previous work (Timotius et al, 2019), we observed that this material can be used as a drug delivery system. We also observed a compatible mathematical model of drug release kinetics in this system (Timotius et al., 2020).

Considering that this material has been extensively studied, in this study, a CgM film was synthesized and characterized as a potential pH-responsive material. The drug release study was conducted at various pH values. A mathematical model was derived, involving several adsorption isotherm models, such as the thermodynamic equilibrium model, namely the Henry model, Langmuir model, and Freundlich model. The moving boundary caused by the film degradation was also involved in the model. Curcumin was used as the drug model in the drug release study and was identified as a cancer medicine.

2. Methods

2.1. Materials

Low-molecular-weight CTS (50–190 kDa, 75–85% DD) was obtained from Sigma Aldrich, USA. Acetic acid (100%) was supplied by Merck, Germany. MA (>99% purity) was purchased from Nacalai Tesque Inc., Japan. Curcumin was purchased from Bio Basic, Inc., Canada. Tween 80 and citric acid buffer solution (pH 2, 4, and 6) were supplied by Merck, Germany. All reagents were used without further purification or treatment.

2.2. Film Preparation

A CgM film was synthesized based on our previous study with slight modification (Timotius et al., 2020). Approximately 2 g of CTS was dissolved in 100 mL of acetic acid (1% v/v). In different glasses, MA (1, 2, and 4 g) was pounded and dissolved in ethanol (70% v/v). The MA solution was then poured into the CTS solution and constantly stirred for 24 h under atmospheric conditions. Then, the unreacted maleic acid was removed through dialysis, which was conducted using a cellulose membrane (MWCO 15 kDa) in ±4 L of Aquadest for 24 h at 4°C. The dialyzed solution was cast on a polyethylene petri dish and

dried at 50°C for 24 h. The samples were encoded as CgM-xy, where x and y represent the masses of MA and CTS, respectively. As the standard, a pure CTS film was synthesized using the same method but without the addition of MA; it was encoded as CTS. All these films were further characterized using Fourier transform infrared (FTIR) spectroscopy. The films were scanned by SHIMADZU IR Prestige-21 in the range of 400– 4000 cm^{-1}. The samples were scanned in the solid state using KBr pellets with 10 scans and 4 cm^{-1} resolution.

2.3. Drug Loading

Drug loading was performed after the dialysis process. The dialyzed solution was mixed with Tween 80 (70% weight Tween 80/weight CTS). Then, curcumin was dispersed and stirred until the solution became homogeneous. Next, the drug-loaded solution was cast on a polyethylene petri dish and dried at 50 °C for 24 h.

2.4. Mechanical Strength

Mesdan Lab Tenso 300 (Type 168E, Serial Number: 397, Salo, Italy) was used to determine the tensile strength and elongation at break of the samples. Each sample was tested 3 times. The films were cut into 2.5 cm × 10 cm and the thickness was determined before mechanical strength measurement. Each sample was pulled at a constant rate (196.5 mm/min) under 300 N load.

2.5. Swellability

The samples (Ø10 mm) were dried at 50 °C in the oven. The dried films were weighed (W_0, g) and then immersed in 50 mL of buffer solution (pH 2, 4, 6, and 7.4). After a certain time interval, the films were taken out and the remaining water on the surface was removed gently. These swelled films were weighed (W_s, g). The equilibrium swellings ratio (Q_e, %) was calculated as using Equation 1.

$$Q_e = \frac{W_s}{W_0} \times 100\% \tag{1}$$

2.6. Degradation Measurement

The dried films were immersed in the buffer solution (50 mL). After that, the films were dried and followed by weighing (Imani et al., 2021, Nadia et al., 2021). The step was repeated in a specific time interval. The drug release analysis was conducted at different pH values (2, 4, 6, and 7.4). The degree of degradation of all samples was calculated using Equation 2 where the W_D (g) was the dried sample after immersion.

$$Degradation(\%) = \frac{W_D}{W_0} \times 100\% \tag{2}$$

2.7. Drug Release

This study was conducted at various pH values (2, 4, 6, and 7.4). The drug-loaded films (Ø10 mm) were immersed in of buffer solution (50 mL). The concentration of the solution was analized using spectrophotometer (Genesys-20) in a certain time interval.

2.8. Kinetics Model

The drug release system is illustrated in **Figure 1** and **Figure 2**. The diffusion of the drug through the matrix film was determined from the following partial differential equation as expressed in Equation 3.

$$\frac{\partial^2 C_A}{\partial z^2} = \frac{1}{D_e} \frac{\partial C_A}{\partial t} \tag{3}$$

where $C_A(z,t)$ is the concentration of curcumin in the matrix film (mg/cm^3), and D_e indicates the effective diffusivity of the matrix film (cm^2/min). The position and time were

labeled as z and t, respectively. There were second-order derivatives with respect to position and first-order derivatives with respect to time; therefore, we would need one initial condition and two boundary conditions as written in Equation 4, 5, and 6 respectively.

$$C_A(z,0) = C_{A0} \tag{4}$$

$$\frac{\partial C_A}{\partial z}(0,t) = 0 \tag{5}$$

$$\frac{\partial C_A}{\partial z}(L^*,t) = \frac{k_{C_A}}{D_e}\left(C_A^*(t) - C_{Af}(t)\right) \tag{6}$$

where C_{A0} and C_{Af} are the initial concentrations of curcumin in the matrix film and bulk liquid, respectively (mg/cm^3), and $L^*(t)$ indicates the half thickness of the film (it decreases with time because of degradation). The variable k_{C_A} is the convection mass transfer constant (cm/min), and C_A^* is the concentration of curcumin in the liquid present on the matrix film surface (mg/cm^3).

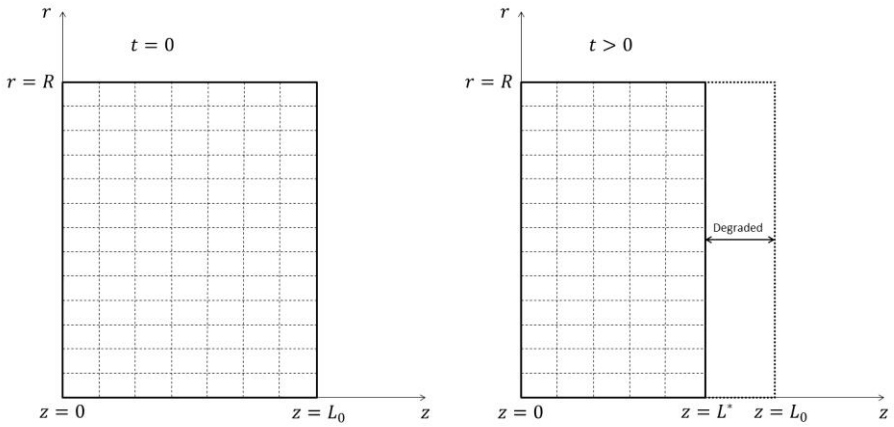

Figure 1 Illustration of Film Degradation that causes the Moving Boundary Case

The correlation between the curcumin concentrations on the film surface in the solid phase ($C_A(L^*,t)$) and liquid phase ($C_A^*(t)$) can be described using an adsorption isotherm. In this study, we used three mathematical models for the adsorption isotherm (i.e., Henry, Langmuir, and Freundlich), as described in Equations 7, 8, and 9, respectively.

$$C_A(L^*,t) = H.C_A^*(t) \tag{7}$$

$$C_A(L^*,t) = \frac{K_L.C_m.C_A^*(t)}{1 + K_L.C_A^*(t)} \tag{8}$$

$$C_A(L^*,t) = K_f.\left(C_A^*(t)\right)^n \tag{9}$$

In the drug release study, the measured curcumin concentration was in the bulk liquid. Hence, the result of $C_A(z,t)$ can be transformed into C_{Af} as expressed in Equation 10.

$$C_{Af}(t) = \frac{2.S}{V}\left(L_0.C_{A0} - \int_0^{L^*} C_A(z,t)dz\right) \tag{10}$$

All parameters were obtained by minimizing the sum of squares of error (SSE), which was calculated using Equation 11. We conducted minimization by using MATLAB to obtain all parameters (D_e, k_{C_A}, H, K_L, C_m, K_f, and n) (Timotius, 2020).

$$SSE = \sum_{i=1}^{i=n} \left(C_{Af}^{expt}(i) - C_{Af}^{calc}(i) \right) \tag{11}$$

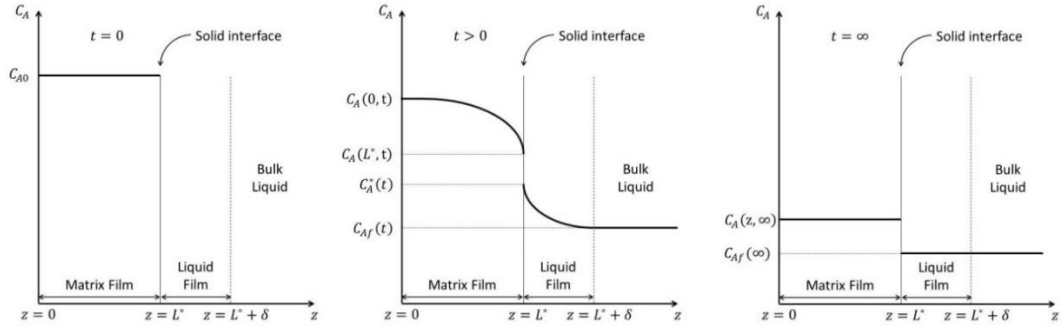

Figure 2 Illustration of the Mass Transfer from the Matrix Film to the Bulk Liquid

3. Results and Discussion

3.1. FTIR Analysis

In this study, CTS and dialyzed CgM-42 were scanned using FTIR to observe the shifting or appearance of any new peaks (Krisanti et al., 2019). The results of both samples are presented in **Figure 3**. The CTS film shows characteristics of CTS spectra. The wide bands at approximately 3448 cm^{-1} correspond to the hydrogen bonds of amines. The amide I (C=O) and amide II (C-N) peaks appear at 1658 and 1558 cm^{-1}, respectively (Kusumastuti et al., 2017b). The amide band appears because CTS is not 100% deacetylated. Then, the existence peaks at 1373 and 1080 cm^{-1} are attributed to the stretching of the amide III (C-N) and C-O-C bands, respectively.

The reaction between CTS and MA follows both amidation and esterification mechanisms (Timotius et al., 2020). This creates new peaks in the CgM-42 film at 1705 and 1573 cm^{-1}, which correspond to the carboxyl group (C=O) and vinyl group (C=C) of the grafted MA, as shown in **Figure 3**. There are also some shifts at amide I and amide II, as well as increased intensity at amide III (1365 cm^{-1}) and C-O-C (1072 cm^{-1}) caused by the MA grafted on the amine group and hydroxyl group of CTS. This result shows that the CgM film is successfully synthesized.

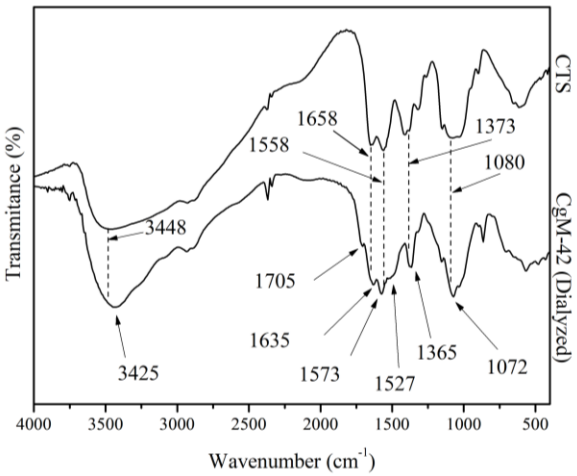

Figure 3 FTIR Results of the CTS and Dialyzed CgM-42 Film

3.2. Acidic Content

It is important to measure the acidic content of all films because it represents the amount of acid in the films. The acidic content of CTS represents the amount of protonated amine groups, while in CgM, the samples are assumed to be proportional to the amount of

grafted MA (Timotius et al., 2019). **Figure 4a** shows the acidic content of each sample for both dialyzed and undialyzed CgM films. The higher acidic content of the undialyzed film corresponds to the appearance of unreacted MA. As the samples are dialyzed, the acidic content of each CgM film decreases. This is because the unreacted MA is removed. This result agrees with that obtained by Vasi et al. (2014). As the grafting is increased, the acid content also increases. The grafted substance is an acid molecule.

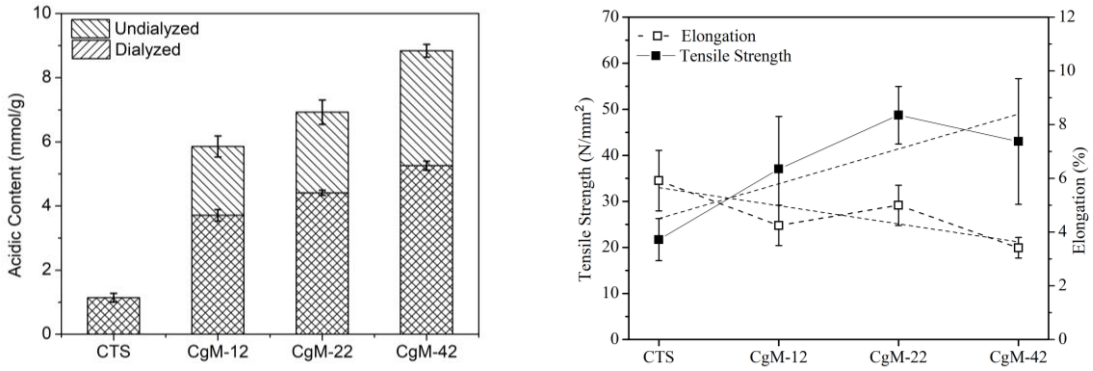

Figure 4 Acidic Content (a) and Mechanical Properties (Tensile Strength and Elongation at Break) (b) of Each Sample

3.3. Mechanical Strength

The tensile strength and elongation at break of each sample are displayed in **Figure 4b**. This measurement is performed to observe the effect of grafting MA on the mechanical strength of the film. The tensile strength of CTS observed in this study is slightly higher than that observed previously (Pereda et al., 2011), which is attributable to the different values of deacetylation and drying processes which has positive effect to the tensile strength (Homez-Jara et al., 2018). They (Pereda et al., 2011) dried the film at 35°C which give tensile strength value at 17.34±2.43 N/mm^2. The low elongation at breaks is typically caused by the properties of CTS, which is known as a stiff material (Escárcega-Galaz et al., 2018).

The results of the mechanical strength measurement show that a higher MA concentration tends to increase the tensile strength and decrease the elongation. This means that the existence of maleic acid on the chitosan backbone creates a crosslinking effect (Zurick & Bernards, 2014) due to the presence of carboxyl groups (negatively charged functional groups) and amine groups (positively charged functional groups). An increased concentration of grafted MA in the film is expected to increase the density of negative charges in the film and lead to increased physical crosslinking.

3.4. Swellability

We observe the swellability of each sample at various pH values, which is an important method to observe the IEP of a polyampholyte. This method is also used to determine which ratio yields polyampholyte properties. The swellability of each sample in various pH environments is presented in **Table 1**, where the symbol "+" indicates soluble, "±" indicates partially soluble (break into small pieces), and "o" indicates swollen.

Table 1 Swellability of Each Sample in Various pH Environments

Samples	pH 2	pH 4	pH 6	pH 7.4
CTS	+	+	±	o
CgM–12	+	±	o	o
CgM–22	±	±	o	o
CgM–42	o	o	o	o

The swellability of the CTS film can be explained by its solubility. CTS is highly soluble in acidic solutions (Rinaudo et al., 1999). As we do not use any crosslinker in the CTS film, it is reasonable to assume that the CTS film is only swollen at a pH of 7.4. However, with the introduction of MA into the CTS backbone, the film tends to be swollen. This occurs because of the physical crosslinking, as explained before, and this result agrees with the mechanical strength result. As presented in **Table 1**, all samples are swollen at pH 7.4, which means that the amine groups of CTS do not react at all with the MA. If the MA:CTS ratio is increased to approximately 3.5:1, it can lead to the formation of water-soluble CTS (Zhou et al., 2017).

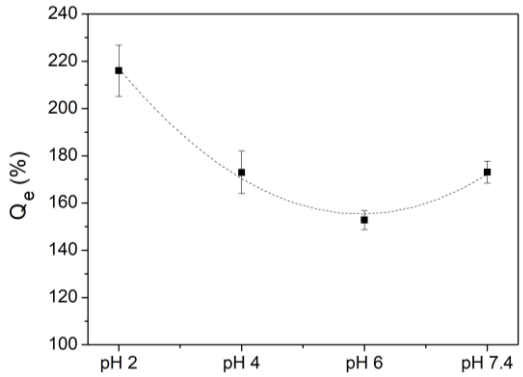

Figure 5 Equilibrium Swelling Ratio of CgM-42 at Various pH Values

Figure 5 shows the equilibrium swelling results of CgM-42 at various pH values. This observation is conducted to identify the IEP of CgM-42. The number of deprotonated carboxyl groups from grafted MA is the same as that of protonated amine groups from CTS (Zurick & Bernards, 2014). This phenomenon causes an attraction between the positive and negative charges and decreases the swelling ratio.

According to the experimental result, the IEP of CgM-42 appears at pH 6. When the pH is below 6, the amine groups are protonated. This makes the film rich in positive charges and creates repulsion between the positive charges. At pH 7.4, the carboxyl groups from grafted MA are deprotonated and create many negative charges. This also produces the repulsion effect and increases the equilibrium swelling ratio (Qian et al., 2019).

3.5. Degradation and Drug Release Study

The rate of degradation is an important factor in this study as it forms the base for the moving boundary case. An empirical model is used as the model for the degradation rate, as shown in Equation (12). Here, m_P, m_0, and t represent the film mass at each time point, initial mass of the film, and time (min), respectively, while a_0 and a_1 are constants. The obtained constant values are presented in **Table 2**. When the degradation is large enough, it affects the drug release rate. The degradation of the polymer also releases the drugs that are entrapped in the matrix. In our experiment, the samples retain their shape; it is assumed that erosion only occurs in the axial direction. Therefore, by using mass conservation, Equation (12) can be modified into Equation (13), where L and L_0 represent the film thickness each time point and the initial thickness of the film, respectively. It is used to determine the film thickness as a function of time.

$$m_p = m_0 \times a_0\left(1-\exp\left(-a_1 \times t\right)\right) \tag{12}$$

$$L = L_0 \times a_0\left(1-\exp\left(-a_1 \times t\right)\right) \tag{13}$$

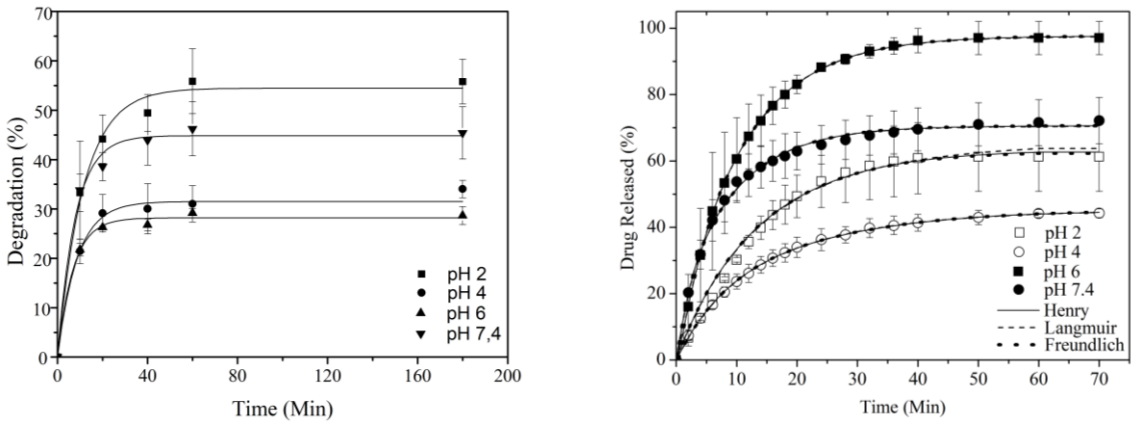

(a) (b)

Figure 6 Degradation Rate (a) and Drug Release Study (b) on CgM-42 at Various pH Values.

The degradation of CgM-42 at various pH values is presented in **Figure 6a**. This result agrees with that obtained for the equilibrium swelling ratio. The polymer degradation is the lowest at the IEP of CgM-42. This result is consistent with the equilibrium swelling ratio result, which is attributable to the fact that the interaction between the positive and negative charges can maintain the entanglement of the chains. Meanwhile, pH values lower and higher than the IEP show that the degradation decreases more than at IEP. This is attributable to the repulsion of the same charge, which implies the disentanglement of the polymer chains (Kono et al., 2013).

A drug release study was conducted for 70 min to observe the behavior of curcumin release at several pH values from CgM-42. The parameters are obtained using SSE minimization in MATLAB©, and the results are presented in **Table 2**. The fittings between the data and Equation (10) are presented in **Figure 6b**. Unlike the degradation and swelling equilibrium, the results of the drug release study show different trends. This can be explained by the charge of the film and the drug model. Curcumin, as the drug model, has two structural forms depending on the medium in which it is present: keto form and enol form. In acidic and neutral media, curcumin appears in the keto form and acts as a proton donor (Singh et al., 2017). The film is dominated by a positive charge at pH values below the IEP, and vice versa (Kono et al., 2013). Therefore, if the pH value decreases, the released curcumin is expected to be lower. In an acidic environment, the film has more positive charges, while curcumin is negatively charged. This means that curcumin has many active sites, which can hold curcumin in the film. However, there is an anomaly at pH 2, which releases more curcumin than at pH 4. This result might have been influenced by polymer erosion. The polymer erosion at pH 2 is greater than that at pH 4. This explains why this phenomenon occurs. At the IEP, curcumin is almost completely released. This occurs because the film has almost neutral net charges, which has been explained by the swelling result.

The results of D_e for all pH and equilibrium models are in the order of magnitude 10^{-7} cm^2/min. This results is consistent with that obtained previously (Timotius et al., 2020). In our previous study, the same order of magnitude of approximately 10^{-7} cm^2/min for the same ratio of MA:CTS at pH 7.4 was obtained, while the order of magnitude for the pure CTS film was 10^{-5} cm^2/min. This means that the release of curcumin from the CgM-42 film is more controlled than that from the pure CTS film. This indicates that D_e is not much affected by the pH value.

Table 2 Parameter Values of Each Equilibrium Model at Various pH Values

	Parameters	pH 2	pH 4	pH 6	pH 7.4
Henry	D_e, cm²/min	2.94×10^{-7}	4.15×10^{-7}	6.32×10^{-7}	2.95×10^{-7}
	k_c, cm/min	7.30×10^{-3}	1.28×10^{-2}	2.23×10^{-3}	1.68×10^{-1}
	H	6.99×10^{3}	9.96×10^{3}	1.76×10^{2}	4.21×10^{3}
	SSE	2.10×10^{-6}	3.46×10^{-8}	8.59×10^{-8}	5.19×10^{-7}
Langmuir	D_e, cm²/min	3.66×10^{-7}	4.15×10^{-7}	6.37×10^{-7}	3.08×10^{-7}
	k_c, cm/min	4.78×10^{-3}	1.27×10^{-2}	1.74×10^{-3}	1.43×10^{-1}
	C_m, mmol/g	1.78×10^{2}	3.00×10^{1}	1.20×10^{0}	4.70×10^{0}
	k_L, L/mmol	2.65×10^{-2}	2.64×10^{-1}	1.22×10^{-1}	7.42×10^{-1}
	SSE	2.15×10^{-6}	3.46×10^{-8}	8.66×10^{-8}	5.28×10^{-7}
Freundlich	D_e, cm²/min	2.71×10^{-7}	2.45×10^{-7}	6.33×10^{-7}	2.99×10^{-7}
	k_c, cm/min	8.33×10^{-3}	1.79×10^{-2}	2.29×10^{-3}	1.60×10^{-1}
	k_f	1.92×10^{4}	1.42×10^{4}	1.86×10^{2}	7.64×10^{3}
	n	3.80×10^{-1}	7.23×10^{-1}	9.71×10^{-1}	5.55×10^{-1}
	SSE	2.11×10^{-6}	3.94×10^{-8}	8.64×10^{-8}	5.24×10^{-7}
	a_0	5.45×10^{-1}	3.15×10^{-1}	2.82×10^{-1}	4.49×10^{-1}
	a_1, min⁻¹	8.68×10^{-2}	1.15×10^{-1}	1.44×10^{-1}	1.26×10^{-1}

The values of the equilibrium parameters are affected by the pH value. This is most likely related to the charge density of the film and curcumin, as explained above. In this study, Henry constants vary by approximately 10^2–10^3 in the order of magnitude. This constant explains the proportional concentration of curcumin in the solid state (film) and liquid state (buffer solution) (Frenning & Strømme, 2003). However, this constant is only applicable at low concentrations (Ayawei et al., 2017). In the Langmuir model, the parameters are C_m and k_L, which indicate the maximum adsorption capacity at full monolayer coverage and the Langmuir constant, respectively (Varnier et al., 2018). In the Freundlich model, k_f and n are the relative adsorption capacity and energy of adsorption, respectively (Proctor & Toro-Vazquez, 2009). The trend of maximum adsorption capacity (C_m and k_f) is consistent with that of the charge density. The adsorption capacity of curcumin increases at pH values below the IEP and decreases as the pH values increase. The increasing intensity of the adsorbent–adsorbate is indicated by the decreasing n value, which is favorable between 0.1 and 1 (Varnier et al., 2018). When the n value approaches 1, the adsorption energy distribution is uniform. It occurs at the IEP, where the active sites are few; therefore, the energy is distributed uniformly. Apparently, all adsorption isotherm models can fit the data, as the curcumin concentration is sufficiently low in this study; however, each model explains a different meaning.

4. Conclusions

The grafting of MA and CTS is successfully performed in this study. Increasing the MA:CTS ratio leads to an increase in the tensile strength and a reduction in the elongation at break. The MA:CTS ratio that results in polyampholyte properties is obtained at 2:1 (w/w) and is denoted as CgM-42. The IEP of CgM-42 is identified at pH 6, which is obtained from the equilibrium swelling ratio study. The degradation behavior is consistent with the swelling result. In the drug release study, all adsorption isotherm models fit the data. The value of D_e is not affected by the pH. However, the adsorption equilibrium parameters are strongly influenced by the pH. The D_e value varies from 2.71×10^{-7} to 6.37×10^{-7} cm²/min.

The Henry constants vary by approximately 10^2 to 10^3 in the order of magnitude, and the Langmuir maximum adsorption capacity is approximately 10^0 to 10^2 mmol/g. The trend of C_m is consistent with the equilibrium swelling ratio. These results show that this film can be used for pH-responsive drug delivery systems.

Acknowledgements

This study was funded by the Ministry of Education and Culture of Indonesia in the scheme of PDUPT with contract number no 2846/UN1.DITLIT/DIT-LIT/PT/2020.

References

Ayawei, N., Ebelegi, A.N., Wankasi, D., 2017. Modelling and Interpretation of Adsorption Isotherms. *Journal of Chemistry*, Volume 2017, pp. 3039817

Escárcega-Galaz, A.A., Sánchez-Machado, D.I., López-Cervantes, J., Sanches-Silva, A., Madera-Santana, T.J., Paseiro-Losada, P., 2018. Mechanical, Structural and Physical Aspects of Chitosan-Based Films as Antimicrobial Dressings. *International Journal of Biological Macromolecule*, Volume 116, pp. 472–481

Frenning, G., Strømme, M., 2003. Drug Release Modeled by Dissolution, Diffusion, and Immobilization. *International Journal of Pharmaceutics*, Volume 250(1), pp. 137-145

Hasipoglu, H.N., Yilmaz, E., Yilmaz, O., Caner, H., 2005. Preparation and Characterization of Maleic Acid grafted Chitosan. *International Journal of Polymer Analysis and Characterization*, Volume 10(5-6), pp. 313–327

Homez-Jara, A., Daza, L.D., Aguirre, D.M., Muñoz, J.A., Solanilla, J.F., Váquiro, H.A., 2018. Characterization of Chitosan Edible Films Obtained with Various Polymer Concentrations and Drying Temperatures. *International Journal of Biological Macromolecule*, Volume 113, pp. 1233–1240

Imani, N.A.C., Kusumastuti, Y., Petrus, H.T.B.M., Timotius, D., Kobayashi, M., 2021. Enhanced Mechanical Properties of Organic-Inorganic Chitosan/Nano Silica Composite Film. *Journal of Advanced Manufacturing Technology*, Volume 15(2), pp. 1–10

Kono, H., Oeda, I., Nakamura, T., 2013. The Preparation, Swelling Characteristics, and Albumin Adsorption and Release Behaviors of a Novel Chitosan Based Polyampholyte Hydrogels. *Reactive and Functional Polymers*, Volume 73(1), pp. 97–107

Krisanti, E.A., Hijrianti, N., Mulia, K. 2019. Preparation and Evaluation of Alginate-Chitosan Matrices Loaded with Red Ginger Oleoresin Using the Ionotropic Gelation Method. *International Journal of Technology*, Volume 10(8), pp. 1513–1522

Kusumastuti, Y., Petrus, H.T.B.M., Yohana, F., Buwono, A.T., Zaqina, R.B., 2017a. Synthesis and Characterization of Biocomposites based on Chitosan and Geothermal Silica. *In:* AIP Conference Proceedings, Volume 1823(1), pp. 020127

Kusumastuti, Y., Shibasaki, Y., Hirohara, S., Kobayashi, M., Terada, K., Ando, T., Tanihara, M., 2017b. Encapsulation of Rat Bone Marrow Stromal Cells using a Poly-Ion Complex Gel of Chitosan and Succinylated Poly (Pro-Hyp-Gly). *Journal of Tissue Engineering and Regenerative Medicine*, Volume 11(3), pp. 869–876

Manga, R.D., Jha, P.K., 2017. Mathematical Models for Controlled Drug Release Through pH-Responsive Polymeric Hydrogels. *Journal of Pharmaceutical Science*, Volume 106(2), pp. 629–638

Morgado, P.I., Aguiar-Ricardo, A., Correia, I.J., 2015. Asymmetric Membranes as Ideal Woun Dressings: An Overview on Production Methods, Structure, Properties, and Performance Relationship. *Journal of Membrane Science*, Volume 490, pp. 139–151

Muharam, Y., Purwanto, W.W., Mulia, K., Wulan, P.P.D.K., Marzuki, I., Dewi, M.N. 2015. Mathematical Model Controlled Potassium Chloride Release Systems from Chitosan Microspheres. *International Journal of Technology*, Volume 6(7), pp. 1228–1237

Nadia, M., Kusumastuti, Y., Wirawan, S.K., Timotius, D., 2021. Effect of Ceric (IV) Ammonium Nitrate Concentration on Preparation and Characterization of Chitosan-graft-Maleic Anhydride as Potential Drug Delivery System. *AIP Conference Proceedings*, Volume 2338(1), pp. 020003

Pereda, M., Ponce, A.G., Marcovich, N.E., Ruseckaite, R.A., Martucci, J.F., 2011. Chitosan-gelatin Composites and Bi-Layer Films with Potential Antimicrobial Activity. *Food Hydrocolloids,* Volume 25(5), pp. 1372–1381

Proctor, A., Toro-Vazquez, J.F., 2009. *The Freundlich Isotherm in Studying Adsorption in Oil Processing*. 2nd Edition. USA: American Oil Chemists' Society

Qian, C., Zhang, T., Gravesande, J., Baysah, C., Song, X., Xing, J., 2019. Injectable and Self-Healing Polysaccharide-Based Hydrogel for pH-Responsive Drug Release. *International Journal of Biological Macromolecules*, Volume 123, pp. 140–148

Rinaudo, M., Pavlov, G., Desbrie, J., 1999. Influence of Acetic Acid Concentration on the Solubilization of Chitosan. *Polymer*, Volume 40(25), pp. 7029–7032

Singh, R.P., Gangadharappa, H.V., Mruthunjaya, K., 2017. Phospholipids: Unique Carriers for Drug Delivery Systems. *Journal of Drug Delivery Science and Technology*, Volume 39, pp. 166–179

Su, E., Okay, O., 2017. Polyampholyte Hydrogels Formed via Electrostatic and Hydrophobic Interactions. *European Polymer Journal*, Volume 88, pp. 191–204

Timotius, D., 2020. Karakterisasi dan Pemanfaatan Chitosan-Graft-Maleic sebagai pH Responsive Drug Delivery System *(Characterization and Utilization of Chitosan-Graft-Maleic sebagai pH Responsive Drug Delivery System)*, Master's Thesis, Graduate Program, Universitas Gadjah Mada, Yogyakarta, Indonesia

Timotius, D., Kusumastuti, Y., Imani, N.A.C., Rochmadi. Putri, N.R.E., Rahayu, S.S., Wirawan, S.K., Ikawati, M., 2020. Kinetics of Drug Release Profile from Maleic-Anhydride-grafted-Chitosan Film. *Materials Research Express*, Volume 7(4), p. 046403

Timotius, D., Rochmadi, Kusumastuti, Y., 2019. Preparation and Characterization of Local Indonesian Chitosan-graft-Maleic Anhydride as Drug Carrier. *In:* IOP Conference Series: Materials Science and Engineering, Volume 599, p. 012029

Varnier, K., Vieira, T., Wolf, M., Belfiore, L.A., Tambourgi, E.B., Paulino, A.T., 2018. Polysaccharide-based Hydrogels for the Immobilization and Controlled Release of Bovine Serum Albumin. *International Journal of Biological Macromolecule*, Volume 120(Part A), pp. 522–528

Vasi, A.M., Popa, M.I., Butnaru, M., Dodi, G., Verestiuc, L., 2014. Chemical Functionalization of Hyaluronic Acid for Drug Delivery Applications. *Materials Science and Engineering C*, Volume 38(1), pp. 177–185

Wibowo, A., Jatmiko, A., Ananda, M.B., Rachmawati, S.A., Ardy, H., Aimon, A.H., Iskandar, F. 2021. Facile Fabrication of Polyelectrolyte Complex Nanoparticles Based on Chitosan – Poly-2-Acrylamido-2-Methylpropane Sulfonic Acid as a Potential Drug Carrier Material. *International Journal of Technology*, Volume 12(3), pp. 561–570

Zurick, K.M. Bernards, M., 2014. Recent Biomedical Advances with Polyampholyte Polymers. *Journal of Applied Polymers Science*, Volume 40069, pp. 1–9

Zhang, J., Jiang, X., Wen, X., Xu, Q., Zeng, H., Zhao, Y., Liu, M., Wang, Z., Hu, X., Wang, Y., 2019. Bio-Responsive Smart Polymers and Biomedical Applications. *Journal of Physics: Materials*, Volume 2(3), p. 032004

Zhou, Y., Dong, Q., Yang, H., Liu, X., Yin, X., Tao, Y., Bai, Z., Xu, W., 2017. Photocrosslinked Maleilated Chitosan/Methacrylated Poly (Vinyl Alcohol) Bicomponent Nanofibrous Scaffolds for use as Potential Wound Dressings. *Carbohydrate Polymers*, Volume 168, pp. 220–226